

# A simple fitting method (*gfit*) for galaxy shape measurement in weak lensing surveys

M. Gentile<sup>1</sup>, F. Courbin<sup>1</sup> and G. Meylan<sup>1</sup>

Laboratoire d'astrophysique, Ecole Polytechnique Fédérale de Lausanne (EPFL), Observatoire de Sauverny, CH-1290 Versoix, Switzerland

Submitted to A&A

## ABSTRACT

It is anticipated that the large sky areas covered by planned wide-field weak lensing surveys will reduce statistical errors to such an extent that systematic errors will instead become the dominant source of uncertainty. It is therefore crucial to devise numerical methods to measure galaxy shapes with the least possible systematic errors. We present a simple "forward deconvolution" method, *gfit*, to measure galaxy shapes given telescope and atmospheric smearings, in the presence of noise. The method consists in fitting a single 2D elliptical Sérsic profile to the data, convolved with the point spread function. We applied *gfit* to the data proposed in the GRavitational lEnsing Accuracy Testing 2010 (GREAT10) Galaxy Challenge. In spite of its simplicity, *gfit* obtained the lowest additive bias ( $\sqrt{\mathcal{A}} = 0.057 \times 10^{-4}$ ) on the shear power spectrum among twelve different methods and the second lowest multiplicative bias ( $M/2 = 0.583 \times 10^{-2}$ ). It remains that *gfit* is a fitting method and is therefore affected by noise bias. However, the simplicity of the underlying galaxy model combined with the use of an efficient customized minimization algorithm allow very competitive performances, at least on the GREAT10 data, for a relatively low computing time.

**Key words.** Gravitational lensing: weak – Methods: data analysis

## 1. Introduction

Weak gravitational lensing (e.g., Bartelmann & Schneider 2001; Hoekstra & Jain 2008), whereby the gravitational bending of light by structures in the Universe slightly distorts images of distant galaxies, is now recognized as a powerful means to study the history of the Universe and probe the mysterious nature of the dark matter and dark energy (Munshi et al. 2008; Huterer 2010).

Since the first detection of weak lensing (Maoli et al. 2001; Bacon et al. 2000; Kaiser et al. 2000; Van Waerbeke et al. 2000; Wittman et al. 2000), a number of methods have been devised and implemented to tackle the inverse problem of recovering the lensing signature from observed, distorted galaxy images (Kaiser et al. 1995; Luppino & Kaiser 1997; Hoekstra et al. 1998; Bernstein & Jarvis 2002; Hirata & Seljak 2003; Refregier & Bacon 2003; Heymans et al. 2006; Massey et al. 2007; Miller et al. 2007; Kitching et al. 2008; Bridle et al. 2010; Kitching et al. 2012).

We describe in this paper *gfit*, a simple shear measurement method that nevertheless obtained good results in the latest GRavitational lEnsing Accuracy Testing 2010 (GREAT10) Galaxy challenge (Kitching et al. 2011, 2012). Galaxies are assumed to be well modeled by a seven-parameter, single-component elliptical Sérsic profile. The shape measurement algorithm essentially consist in iteratively shearing and convolving the galaxy model until a sufficiently close match with the observed galaxy is reached. Instead of an out-the-box minimizer, we employ a custom-developed minimizer well suited to fitting faint and noisy images like those frequently found in weak lensing.

The paper is structured as follows. We provide in Sect. 2 a description of the underlying principles, galaxy model and shape measurement algorithm of *gfit*. We continue in Sect. 3 with a pre-

sentation of the pipeline we used to participate in the GREAT10 Galaxy challenge and follow with a analysis of the *gfit* results in Sect. 4. We conclude in Sect. 5.

## 2. The *gfit* shear measurement method

### 2.1. The shear measurement problem

According to the theory of weak gravitational lensing, the light emitted by a galaxy is slightly deviated by the foreground gravitational field, an effect that can be modeled to first order as the combination of two effects, the *convergence*  $\kappa$  and the *shear*  $\gamma$ , that describe how light bundles emitted by a source are distorted by a potential well. The convergence models the magnification effect whereby the galaxy image see its apparent size increased without altering its shape, whereas the shear describes a stretching effect where only ellipticity is altered, not size.

All so-called "shear measurement methods" attempt to reconstruct the reduced shear  $g = \gamma/(1 - \kappa - \gamma)$  which is approximately equals to the shear  $\gamma$  in the weak gravitational limit, where  $\kappa \ll 1$  and  $\gamma \ll 1$ .

The lensing effect is very subtle, however, and requires measuring the shapes of thousands of faint galaxies. Moreover, before they reach the observer, the apparent galaxy images undergo a number of additional distortions, unrelated to lensing, that further complicates that task, mainly:

- The convolution of the images by the instrumental and/or atmospheric point spread function (PSF) that flattens and circularizes the galaxy light profile.
- The Gaussian and Poisson noise introduced by the surrounding sky emissions and the detecting device.
- The pixelation effect caused by the integration of light falling on the detector pixels.

The traditional approach for estimating the shear is to measure the deviation from circularity of a large number of galaxy shapes. But this technique assumes the shear remains constant across the field of view, which is generally not the case. Moreover, accurate shear measurement must also account for a spatially varying PSF that must be interpolated at the positions of the galaxies.

A shear measurement pipeline must overcome all the above difficulties, typically going through the following steps:

1. *PSF correction*, whose goal is to restore the shape a galaxy had before being convolved with the PSF. If the spatial variation of the PSF over the field of view is significant, this step also requires interpolating the PSF to the position of the galaxies in the sky.
2. *Shape measurement*, that is, the estimation of the galaxy shape *after* it has been altered by the cosmic shear but *before* PSF convolution and other subsequent distortions. In this paper, we call the corresponding shape the *sheared* galaxy shape. The real galaxy ellipticity prior to gravitational lensing (i.e. unsheared) is referred to as the *intrinsic ellipticity*.
3. *Shear measurement*, that is, the task of extracting the shear signal from the sheared galaxy shapes estimated in the previous step. A spatially-varying shear field is commonly described as a power spectrum or a correlation function.

Additional steps may also be performed to correct the images from the effects of pixelation and noise.

## 2.2. Shear measurement with *gfit*

The *gfit* “galaxy fitting” method grew from a prototype initially developed by Stéphane Paulin-Henrikson on the occasion of the GREAT08 challenge (Bridle et al. 2008), where it obtained the third and fifth ranks on images with high and low signal to noise ratios respectively (Bridle et al. 2010).

The GREAT10 *gfit* code was subsequently made more generic in order to satisfy the more demanding requirements of the Galaxy challenge. It was also enhanced in several aspects that we describe in subsequent sections of this paper.

It is also worth mentioning that a wavelet-based denoising algorithm described in Nurbaeva et al. (2011) was also experimented in the Galaxy challenge and proved quite successful. This denoising scheme is presented in Sect. 2.7.

The overall shape measurement procedure is the following:

1. Application of the denoising algorithm on the galaxy and/or PSF images [optional]
2. Estimation of the galaxy and PSF centroids in all images
3. Application of the PSF correction and shape measurement algorithm
4. Generation of the ellipticity catalogs
5. Production of various statistics and plots for analysis [optional]

We detail in the next sections the shape measurement algorithm along with its underlying models and components.

## 2.3. Modeling the galaxies

*gfit* is fundamentally a model-fitting method. We describe here the model used to represent galaxies and cover the fitting-related

aspects in Sects. 2.4 and 2.5.

Galaxies are assumed to have a surface brightness distribution well described by an elliptical Sérsic function (Sérsic 1968), defined by:

$$I(\xi, n, r_e) = I_{sky} + I_0 \exp \left[ -b_n \left( \frac{\xi}{r_e} \right)^{1/n} \right] \quad (1)$$

where:

- $I_{sky}$  represents the sky brightness
- $I_0$  is the central surface brightness of the galaxy
- $n$  denotes the Sérsic index that determines the degree of curvature of the profile. A small value of  $n$  leads to a less centrally concentrated profile and a shallower logarithmic slope at small radii.
- The scale radius parameter  $r_e$  is defined as the effective radius encircling half of the total light of the profile (e.g. Ciotti 1991; Trujillo et al. 2004; Graham & Driver 2005).
- The factor  $b_n$  (e.g. Ciotti & Bertin 1999) arises from the definition of  $r_e$  and is related to the Sérsic index  $n$  through the equation  $\Gamma(2n) = 2\gamma(2n, b_n)$  where  $\Gamma$  and  $\gamma$  functions are respectively the complete and incomplete gamma functions (Abramowitz & Stegun 1965).
- The parameter  $\xi$  in Eq. (1) is defined as

$$\xi = \sqrt{(x' - x_c)^2 + \frac{(y' - y_c)^2}{q^2}} \quad (2)$$

and denotes the distance from the centroid  $(x_c, y_c)$  of the galaxy to a point on an elliptical isophote at spatial coordinate  $(x', y')$

$$\begin{bmatrix} x' - x_c \\ y' - y_c \end{bmatrix} = \begin{bmatrix} \cos \phi & \sin \phi \\ -\sin \phi & \cos \phi \end{bmatrix} \begin{bmatrix} x - x_c \\ y - y_c \end{bmatrix},$$

obtained after counterclockwise rotation through an angle  $\phi$  with respect to the  $(0, x)$  axis.

- The quantity  $q$  in expression (2) of  $\xi$  is the ratio of the semi-minor axis  $b$  to the semi-major axis  $a$  of the isophote ellipse. It is related to the complex ellipticity  $\mathbf{e} = (e_1, e_2)$  of the galaxy through  $q = b/a = (1 - |\mathbf{e}|)/(1 + |\mathbf{e}|)$  with  $|\mathbf{e}| = \sqrt{e_1^2 + e_2^2}$ ,  $e_1 = |\mathbf{e}| \cos 2\phi$  and  $e_2 = |\mathbf{e}| \sin 2\phi$ .

This model was initially chosen for its simplicity and has the other merit of being relatively easy to fit. A galaxy represented as the sum of a bulge and a disc would be more realistic, but it is not clear whether such a model would prove more accurate on weak lensing images and worth the additional complexity and computational cost, given degeneracies between parameters. As regards *gfit*, the GREAT10 results does not provide a definitive answer (see Sect. 4).

## 2.4. Galaxy shape measurement and PSF correction

We describe in this section the shape measurement algorithm of *gfit*. It is based on iterative fitting of observed galaxies to the galaxy model described in Sect. 2.3. The basic assumptions of the algorithm are the following:

- All galaxy and PSF fields have been reduced and the objects they contained assumed available in the form of square postage stamps in FITS format. We denote by  $O$  a galaxy field image of the GREAT10 Challenge and by  $o$  any of its

10,000 galaxy postage stamps. The GREAT10 PSF field image corresponding to  $O$  is labeled as  $P$  and any of its individual PSF kernel as  $p$ .

- The  $O$  and  $P$  images have been denoised beforehand if requested. The denoising tool described in Sect. 2.7 is the default choice.
- The centroids of all galaxies and PSF to be processed have been estimated. A tool based on SExtractor (Bertin & Arnouts 1996) has been written for this purpose (see Sect. 2.6.)
- The PSF field at the position of each galaxy is known, so that we can always find the PSF  $p$  that matches galaxy  $o$ .

The fitting algorithm itself is summarized below:

- For each galaxy object  $o$  in observed galaxy field  $O$ 
  - ◊ Extract a square stamp cutout of a given dimension  $N_G \times N_G$  around the centroid  $(x_c, y_c)$  of  $o$ .
  - ◊ Remove the sky background from  $o$  after having estimated its variance  $\sigma_{sky}^2$ .
  - ◊ Estimate the galaxy noise variance  $\sigma^2$  of  $o$ .
  - ◊ Select guess parameters for the 7 model parameters  $\{I_0, (x_c, y_c), (e_1, e_2), n, r_e\}$  described in Sect. 2.3.
  - ◊ Construct an initial galaxy postage stamp  $g$  based on the Sérsic profile having these parameters.
  - ◊ Select the PSF  $p$  that matches the spatial coordinates of  $o$  in  $O$  and extract a cutout of dimension  $N_P \times N_P$  about the centroid. Make sure the PSF is normalized and has the sky background removed.
  - ◊ Iteratively vary the model parameters with the objective of minimizing the residuals between  $g$  and  $o$ .

At each step:

- ⇒ Convolve the model galaxy  $g$  with the observed PSF  $p$  and compute a new galaxy estimate  $k = p \star g$
- ⇒ Compute the residuals between  $o$  and  $k$  using the chi-squared statistics

$$\chi^2 = \sum_n \sum_m \frac{(o_{n,m} - k_{n,m})^2}{\sigma_{n,m}^2}$$

where  $o_{n,m}$  and  $p_{n,m}$  represent the pixel value at position  $(n, m)$  in  $o$  and  $p$  respectively. Similarly,  $\sigma_{n,m}$  denote the standard deviation of the noise associated with each pixel at  $(n, m)$ .

- ⇒ If the minimum  $\chi^2$  has not been reached, select a new set of parameters and construct the corresponding model galaxy  $g$ . Otherwise, exit the minimization loop.

- ◊ At the end of the iteration cycle, the algorithm yields:
  - ⇒ An estimate for all 7 model parameters and for the complex ellipticity  $(e_1, e_2)$  in particular.
  - ⇒ A postage stamp for the best-fitted intrinsic galaxy postage stamp  $g$ .
  - ⇒ A postage stamp for the best-fitted convolved galaxy  $k$ .
- ◊ The same procedure is followed for the next galaxy  $o$  in  $O$ , until all galaxies have been processed.
- Once the shape of all galaxies have been measured, produce a catalog containing the fitted parameters at the positions of the galaxies  $o$  in  $O$  and optionally, additional statistics and plots. Quantities such as the ellipticity modulus  $|\mathbf{e}|$ , the position angle  $\phi$  or the minor-to-major axis ratio  $q$  can be respectively derived from  $(e_1, e_2)$  using  $|\mathbf{e}| = \sqrt{e_1^2 + e_2^2}$ ,  $\phi = \frac{1}{2} \arctan(e_2/e_1)$  and  $q = (1 - |\mathbf{e}|)/(1 + |\mathbf{e}|)$ .

The algorithm just described is not dependent on the galaxy or the PSF model. It would remain unchanged, for instance, if the centroid of the PSF itself was taken into account during fitting or if a bulge and a disc were incorporated in the galaxy model. The quality of the whole shape measurement procedure can thus be increased by improving the models.

The shape measurement algorithm has its own strengths and weaknesses, outlined below:

- Strengths:
  - ◊ Simplicity.
  - ◊ PSF deconvolution and galaxy model estimation are performed simultaneously.
  - ◊ The deconvolution process does not involve any matrix inversion and its side effects (numerical instabilities, presence of artifacts, noise amplification, etc.).
  - ◊ The intrinsic and best-fitted modeled galaxies are obtained as a by-product of the algorithm, in addition to the estimated model parameters.
- Weaknesses:
  - ◊ A bias is introduced through the choice of a galaxy model, which is necessarily imperfect.
  - ◊ The choice of the initial guess parameters of the galaxy model are more or less arbitrary and may also influence the final model parameter estimates:
  - ◊ The algorithm relies heavily on the accuracy and robustness of the minimizer.
  - ◊ The method is sensitive to noise bias
  - ◊ No estimate of errors is available

## 2.5. The *gfit* minimizer

The *gfit* galaxy model expressed by Eq. (1) varies linearly with the parameter  $I_0$ , but non-linearly with the remaining parameters  $\{(x_c, y_c), (e_1, e_2), n, r_e\}$ . This requires the use of a non-linear minimization algorithm over a seven-dimensional parameter space.

Unlike linear minimizations schemes that only involve a matrix inversion, non-linear optimization requires iterating over the parameter space to find the minimum value of the objective function, which is in our case the  $\chi^2$  of the residuals between observed and estimated images. That minimum is not necessarily the absolute minimum of the  $\chi^2$  function but the most relevant from the point of view of the physics of the problem. In our case, the minimum should coincide with the Sérsic model parameters that best fit the galaxy shape.

A good minimizer is essential to any galaxy model fitting algorithm, but finding such a minimum in a reliable manner can prove tricky for a number of reasons:

- Parameter degeneracy, where different combinations of the parameters yield similar  $\chi^2$  values.
- Errors related to noise and undersampling may degrade the accuracy of the fit in several ways: (1) the distortion of the galaxy image may be such that the minimizer fits a wrong shape, even if it does it accurately. (2) The minimizer may be fooled by a “false” local minimum and converge toward wrong fitted parameter values. (3) The minimizer may fail to converge altogether if it cannot reconcile the model with the observed image.
- The choice of initial guess values for the parameters can influence the outcome of the minimization algorithm: depending on the starting location on the parameter hypersurface, the algorithm may tend to follow a different path and converge to a different minimum.

In this regards, the choice of the galaxy model used by *gfit* leads to a number of challenges:

- The total flux  $I_0$  is degenerate with the  $n$  and  $r_e$  parameters, so that, for instance, in Eq. (1), a low  $I_0$  flux may be compensated by a higher exponential function of  $n$ ,  $r_e$  and  $(x_c, y_c)$ , modifying the shape of the fitted galaxy profile. Similarly, an error in the estimation of the sky brightness  $I_{sky}$  may “drive” the minimizer toward a wrong combination of the remaining parameters. This is why we estimate  $I_{sky}$  separately in the algorithm described in Sect. 2.4.
- *gfit* attempts to limit the effect of noise by applying the denoising method described in Sect. 2.7. As regards pixelization, *gfit* can optionally construct the galaxy model in higher resolution and rebin the pixels before fitting.
- To estimate the initial guess values for fitting a particular galaxy, *gfit* can be setup to either accept default values or use estimates from SExtractor.

Several families of optimization algorithms were experimented on GREAT08 and GREAT10 images: simplex (*Nelder-Mead downhill*), gradient descent (*Powell*), Newton & quasi-Newton (*Newton-CG*, *BFGS*) and *Levenberg-Marquardt* (LVM). Descriptions of these algorithms can be found in (e.g. Levenberg 1944; Marquardt 1963; Powell 1964; Nelder & Mead 1965; Zhu et al. 1997; Nocedal & Wright 1999; Bonnans et al. 2006).

None of these methods proved entirely satisfactory, either failing to converge or yielding insufficient accuracy, especially on low signal to noise ratio (S/N) images. The LVM implementation from the SciPy library (Jones et al. 2001–; Community 2010) that we used was the fastest and the most accurate. For these reasons we used it in the GREAT08 version of *gfit*, but that implementation of LVM:

- Failed to converge in about 5-10% of the time on GREAT08 “real noise blind” images.
- Was occasionally tricked by “false” local minima, producing the smallest residuals but with unphysical Sérsic parameters or ellipticities.
- Required good estimates of guess parameters in order to converge towards the right minimum.

We also experimented a parameter estimation scheme based on a Bayesian approach and implemented using the *pymc* Markov Chain Monte Carlo (MCMC) library of Patil et al. (2010), but that method produced less accurate estimates while being less computationally efficient.

In an attempt to overcome these issues, we eventually decided to implement a custom minimizer, better suited to fitting noisy, pixelized galaxy images than vanilla minimization algorithms. We found that a scheme based on an adaptive *cyclic coordinate descent* algorithm (CCD) was able to produce more accurate estimates while at the same time being more robust:

- Able to better cope with degenerate and correlated parameters: LVM has difficulties with the  $\{I_0, n, r_e\}$  degeneracy and coupling and the steepest descent algorithm used in LVM occasionally jumps without precaution to a minimum value that may be the smallest but not the most appropriate one. To avoid this, the CCD algorithm ensures that these parameters are carefully varies in a “round-robin” manner at the beginning of the fitting process, where the amplitudes in variation are the greatest. This scheme is also much more tolerant with regards to initial guess values and converges reliably, making it more robust overall.

- More resilient to noise and on average more accurate than LVM, especially on low S/N images.

The CCD algorithm proved suitable for fitting without any single failure the huge number of GREAT10 galaxies. It nevertheless has a number of drawbacks, namely:

- The convergence rate is lower than that of LVM, resulting in a greater number of function evaluation. It is thus much slower than LVM.
- Its efficiency decreases rapidly with the number of parameters. The algorithm performance is also influenced by factors such as the specific stopping conditions chosen or the range if iteration step sizes specified for the parameters.

The current *gfit* implementation can be configured to use either the CCD, LVM or MCMC-based minimizer.

## 2.6. Centroid estimation

*gfit* does not assume objects to be correctly centered within their postage stamps and accurate estimates for galaxy and PSF objects are required for two main reasons:

- *gfit* does not necessarily use the whole postage stamps for the galaxy and the PSF to save computational time and reduce noise: the corresponding postages stamps are cut out to a smaller dimension (e.g. 24×24 instead of e.g., 48×48 around the estimated centroid).
- The coordinates of the galaxy and PSF centroids are provided to the minimizer as initial guess values before the fitting cycle can begin. Accurate centroids are especially important if the LVM minimization algorithm is used (CCD is much more tolerant in this respect).

*gfit* relies on centroid estimates obtained from the SExtractor tool (Bertin & Arnouts 1996). A catalog is generated with centroid information and additional data such as flux, ellipticities and position angles, that can be optionally used to set guess parameter values.

## 2.7. Denoising

Correcting astronomical images from the effect of noise has always been a challenging task. This is particularly true for galaxy images captured for weak lensing analysis because noise not only degrades the overall quality of these images but also alters the shapes of the galaxies. This causes serious difficulties to all existing shear measurement schemes that found their shear extraction algorithms on the accurate measurement of galaxy shapes.

The challenge is then to correct galaxy images from noise without compromising the shear signal they encode. Unfortunately, popular denoising algorithms based on median filtering (Arce 2005; Arias-Castro & Donoho 2009), Wiener filtering (Wiener 1949; Khireddine et al. 2007) or discrete wavelet transform (DWT) (Bruce et al. 1994; Vetterli & Kovacevic 1995) are not shape preserving and do not meet that requirement.

By default, *gfit* uses *DWT-Wiener*, a shape-preserving denoising technique combining DWT and Wiener filtering developed at the laboratory of astrophysics of EPFL by Nurbaeva et al. (2011). That algorithm has been experimented during the GREAT10 Galaxy challenge and was able to significantly improve the quality factors of all the shear measurement methods from EPFL that participated in the Galaxy challenge (Kitcing

et al. 2012): that was the case for *gfit* but also for *MegaLUT* (Tewes et al. 2012) and *TVNN* (Nurbaeva et al. in prep.).

Interestingly, denoising improves the shape measurement of the three algorithms even though they are fundamentally different from each other.

Beyond shape-preservation, another advantage of the *DWT-Wiener* algorithm lies in its ability to denoise “in one go” images containing a great number of objects, without having to individually process each object in turn. In GREAT10, for instance, *DWT-Wiener* was directly applied to images containing  $100 \times 100$  PSF or galaxy postage stamps.

### 3. Applying *gfit* to the GREAT10 data

#### 3.1. The GREAT10 Galaxy challenge

We describe in this section the specific pipeline we used in the GREAT10 Galaxy Challenge competition that took place between December 2010 and September 2011. The aim, content and rules of the challenge have been described in the GREAT10 Handbook (Kitching et al. 2011, 2012). In a nutshell, the main goals of the GREAT Challenges are (i) to test existing weak lensing measurements methods and (ii) to promote the development of new, more accurate, shear measurement techniques.

The data consist of 24 datasets of 200 simulated galaxy images, each containing 10,000 noisy, PSF-convolved  $48 \times 48$  pixel galaxy postage stamps, arranged on a  $100 \times 100$  grid (see Fig. 1). The GREAT10 edition includes spatially-varying PSF and shear fields, contrary to its predecessor, the GREAT08 challenge (Bridle et al. 2008; Bridle et al. 2010), where these fields were set as constant.

Each of the 24 sets is designed to evaluate the ability of competing methods to deal with galaxy or PSF fields with different properties (e.g. size, signal to noise ratio). We have reproduced in Table 2 the main PSF and galaxy characteristic attached to each of the GREAT10 set, as specified in the Galaxy Challenge results paper (Kitching et al. 2012), Appendix D.

The sets were also classified into “Single epoch”, “Multi-epoch” and “Stable single epoch”, depending on whether the intrinsic ellipticities and PSF keep the same or change their spatial distribution between images in a set (see Table 1).

Participating methods were ranked according to the following metrics :

- A “Raw” quality factor  $Q$  according to which the live leader board was scored and that measures the difference, averaged over all sets, between the reconstructed and true shear power spectra.
- A quality factor  $Q_{dn}$  obtained after estimation and correction of pixel noise.
- A quality factor  $Q_{dn \& \text{train}}$  after application of an additional training step on top of pixel-denoising. That step consists essentially in estimating the multiplicative and additive biases on high S/N galaxy images (set 7) and applying that calibration on the remaining sets.
- A split of the total bias into an shear-independent additive bias and a shear-dependent multiplicative bias between the measured and true shear, respectively denoted as  $c$  and  $m$  where  $c = \langle c_i \rangle$  and  $m = \langle m_i \rangle$ ,  $i = (1, 2)$ . The  $c_i$  and  $m_i$  are respectively the additive and multiplicative biases over the two component of shear  $\gamma_1$  and  $\gamma_2$  and are similar to those used in STEP I (Heymans et al. 2006) and GREAT08 (Bridle et al. 2010) for a constant shear field. They are calculated by

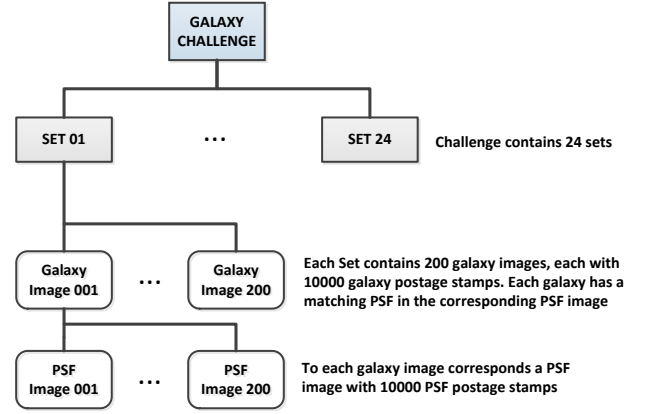


**Fig. 1.** The GREAT10 Galaxy challenge dataset structure. There are 24 galaxy sets, each containing 200 galaxy images with 10000 galaxy postage stamps each. To each galaxy postage stamp corresponds a matching PSF postage stamp at the same spatial position in the galaxy image.

assuming the error on the shear,  $\gamma_i - \gamma_i^{true}$ , and the true shear  $\gamma_i^{true}$  obeys a linear relationship of the form

$$\gamma_i - \gamma_i^{true} = m_i \gamma_i^{true} + c_i \quad (i = 1, 2) \quad (3)$$

More details are provided in Appendix B of (Kitching et al. 2012). See e.g. Huterer et al. (2006) for a discussion on the origin of additive and multiplicative errors in weak lensing studies.

- Additional bias metrics  $\mathcal{A} \simeq \sigma^2(c)$  and  $\mathcal{M} \simeq m^2 + 2m$ , intended to measure the additive and multiplicative biases calculated at power spectrum level. Unlike  $c$  and  $m$ , these metrics account for spatial variability.

#### 3.2. The GREAT10 *gfit* implementation

The GREAT10 version of *gfit* only implements the first two steps described in Sect. 2.1, that is, PSF correction and galaxy shape measurement.

In GREAT10, the estimation of the shear field (third step in Sect. 2.1) was not mandatory as participants were allowed to supply for each image a catalog of estimated galaxy ellipticities instead of a shear power spectrum (Kitching et al. 2011): an analysis program was written by the GREAT10 team to calculate a shear power spectrum from user-supplied ellipticity catalogs. Consequently, like most other competing methods, *gfit* only provided its estimates in the form of a catalog of estimated ellipticities at requested positions within the images. Future version of *gfit* will allow the extraction of a spatially varying shear.

The *gfit* implementation used in GREAT10 consisted of the following stages:

**Table 1.** Spatial variability of PSF and intrinsic ellipticities: images within a set may keep or not the same PSF or intrinsic ellipticity pattern of variation.

Type of variability within a set	PSF	Intrinsic ellipticity
Type 1: “Single epoch”	Variable	Variable
Type 2: “Multi-epoch”	Variable	Fixed
Type 3: “Stable single epoch”	Fixed	Variable

**Table 2.** Some of the PSF and galaxy properties characterizing the GREAT10 image sets. The second and third columns specify whether the PSF or intrinsic ellipticity field were kept constant for all images within a set. The parameters in the fourth column have been detailed in Kitching et al. (2012). The default signal to noise (S/N) ratio is 20, while low and high S/N ratios are 10 and 40 respectively. All sets, except the last four, have galaxies with co-centered bulges and disks with a 50/50 bulge-to-disk ratio.

Set	PSF	Intrinsic ellipticity	Property of images
1	Variable	Variable	Fiducial
2	Fixed	Variable	Fiducial
3	Variable	Fixed	Fiducial
4	Variable	Variable	Low S/N
5	Fixed	Variable	Low S/N
6	Variable	Fixed	Low S/N
7	Variable	Variable	High S/N
8	Fixed	Variable	High S/N
9	Variable	Fixed	High S/N
10	Variable	Variable	Smooth S/N
11	Fixed	Variable	Smooth S/N
12	Variable	Fixed	Smooth S/N
13	Variable	Variable	Small galaxy
14	Fixed	Variable	Small galaxy
15	Variable	Variable	Large galaxy
16	Fixed	Variable	Large galaxy
17	Variable	Variable	Smooth galaxy
18	Fixed	Variable	Smooth galaxy
19	Variable	Variable	Kolmogorov PSF
20	Fixed	Variable	Kolmogorov PSF
21	Variable	Variable	Uniform bulge/disc ratios
22	Fixed	Variable	Uniform bulge/disc ratios
23	Variable	Variable	50/50 bulge/disc offset
24	Fixed	Variable	50/50 bulge/disc offset

1. Optional denoising of the galaxy and PSF images with the DWT-Wiener method presented in Sect. 2.7.
2. Centroid estimation using SExtractor (Bertin & Arnouts 1996) as described in Sect. 2.6.
3. Galaxy shape measurement with the *gfit* program, configured to use the CCD minimization algorithm described in Sect. 2.5. We used  $24 \times 24$  pixel cutouts instead of the full  $48 \times 48$  pixel original galaxy postage stamps. Similarly, the size of PSF postage stamps was reduced to  $12 \times 12$  pixels. That decision was made in order to keep the overall computation time within acceptable limits and avoid picking-up too much noise near the borders of the postage stamps.

Because of the large number of galaxies, running the pipeline on one single processor would not have allowed to meet the GREAT10 deadline. Even with a processing time per galaxy of 0.5 seconds, it would have taken about one month to complete process the full GREAT10 dataset. The ability to simultaneously run multiple program instances use of parallelism is thus imperative and all programs (denoising, SExtractor wrapper, *gfit*) are written to take advantage of parallel computers through the Message Passing Interface (MPI) (Forum 1995, 1998). When only a few processors are required, the same programs can also run on machines with symmetric multiprocessing (SMP) architecture. It took about 5 days to process the entire GREAT10 chal-

**Table 3.** Main metrics for “gfit den” and “gfit” .

Method	$Q$	$Q_{dn}$	$Q_{dn \& \text{train}}$	$M/2 \times 10^{-2}$	$\sqrt{\mathcal{A}} \times 10^{-4}$
gfit den	103.81	197.88	229.19	-2.067	+0.061
gfit	50.11	122.74	249.88	+0.583	+0.057

lenge images on a 64-processor machine, which corresponds to a processing time between 1 and 2 seconds per galaxy.

The pipeline is implemented in Python, a programming language known for its power, flexibility and short development cycle. The usual standard Python libraries are used, notably: NumPy, SciPy, PyFITS and matplotlib. SciPy is the standard scientific library for Python and most of its functions consist of thin Python wrappers on top of fortran, C and C++ functions. SciPy takes advantage of installed optimized libraries such as LAPACK (Linear Algebra PACKage) library (Anderson et al. 1990).

#### 4. Analysis of the gfit GREAT10 results

We summarize and analyze in this section the main Galaxy Challenge results as far as *gfit* is concerned. An overview of the GREAT10 results for available participating shear measurement methods has already been performed in the GREAT10 Galaxy challenge paper (Kitching et al. 2012). Our objective here is to provide a more detailed analysis of the *gfit* results.

We do not, however, analyze the influence of the pixel-denoising and training calibration schemes applied in (Kitching et al. 2012), which we leave for future investigation.

##### 4.1. Overall results

The results of the best 12 methods that participated in the GREAT10 Galaxy Challenge are listed in Table 3 of the Kitching et al. (2012) GREAT10 result paper. That list aggregates results submitted before the official challenge deadline as well as submissions made during the so-called “Post challenge”, a one-week extension to the competition following the deadline.

Two versions of *gfit* were submitted during the challenge, one named “gfit den cs” that included a denoising step using the DWT-Wiener algorithm described in Sect. 2.7 and the other, simply named “gfit”, that did not. The results obtained by both methods are shown in Table 3.

The *gfit* version presented in Kitching et al. (2012) is what we refer to here as “gfit”. In addition, we also present “gfit den cs”, described in Appendix E5 of Kitching et al. (2012) but whose results were not included in the analysis. The “gfit” version is identical except that no denoising was applied to the data before applying the shape measurement algorithm. To simplify, we shorten the name “gfit den cs” to “gfit den” in the remainder of this article.

It can be seen from Table 3 that “gfit den” reaches a raw quality factor  $Q$  twice as high as that of “gfit”. This illustrates the gain in accuracy provided by the DWT-Wiener denoising algorithm. This is further analyzed in Sect. 4.2.2. When the pixel-level denoising algorithm of Kitching et al. (2012) is applied, the  $Q_{dn}$  quality factors of both “gfit” and “gfit den” are improved by a factor  $\sim 2$ , “gfit den” scoring the best  $Q_{dn}$  of all methods ( $Q_{dn} = 197.88$ ). The training calibration further increases both

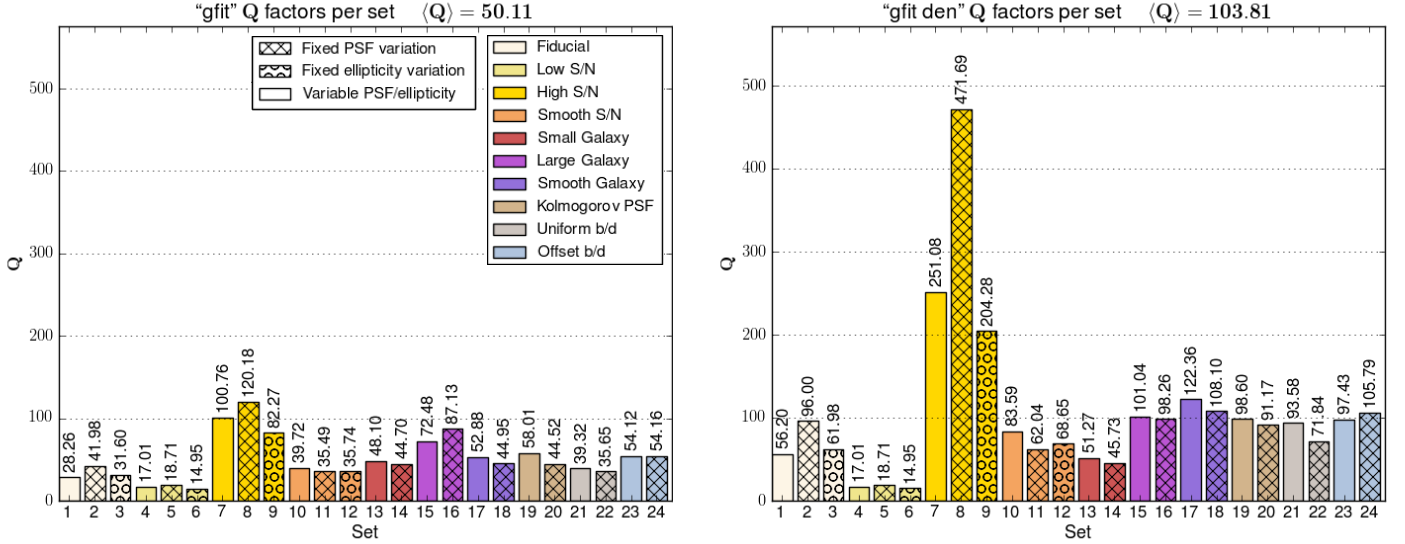


**Fig. 2.** Quality factors per set for “gfit” (left) and “gfit den” (right). The various colors and patterns in the legend indicate the types of features simulated in the sets. The acronyms  $S/N$ ,  $b/d$  respectively refer to the signal to noise ratio and galaxy bulge/disc ratio or offset. The fiducial  $S/N$  was 20 whereas the low  $S/N$  and high  $S/N$  were respectively set to  $S/N = 10$  and  $S/N = 40$ . The labels “Fixed PSF” and “Fixed intrinsic ellipticity” correspond to sets where the PSF and intrinsic galaxy ellipticities were spatially varying across the field but that variation did not change between images within a set. Further details on the structure of the Galaxy challenge dataset and the procedures for calculating the quality factor can be found in in the GREAT10 Galaxy challenge results paper Kitching et al. (2012).

$Q_{dn \& train}$  quality factors, especially that of “gfit” (two-fold increase).

We have also included in Table 3 the average additive and multiplicative biases  $\mathcal{A}$  and  $\mathcal{M}/2$  over all 24 sets. Comparing with Table 3 of the Kitching et al. (2012) result paper, we see that “gfit” reached the lowest average additive bias ( $\sqrt{\mathcal{A}} = 0.057 \times 10^{-4}$ ) and the second lowest average multiplicative bias ( $\mathcal{M}/2 = 0.583 \times 10^{-2}$ ) of all twelve methods (see also the plot in Figure. 1, page 6 of that paper).

We stress that, contrary to what is suggested in Sect. 4.4 of Kitching et al. (2012), the low overall bias of “gfit” is intrinsic to the method and *does not* result from the application of a denoising step. The DWT-Wiener algorithm was only used in “gfit den”, not “gfit” and actually, the average multiplicative bias of “gfit den” ( $\mathcal{M}/2 = -2.067 \times 10^{-2}$ ) is higher than that of “gfit”. Moreover, both methods have similar additive biases. Drawing a more refined conclusion about these biases requires an analysis at individual set level, which we perform in Sect. 4.3.

#### 4.2. Method accuracy

In this section we use the quality factor as a measure of accuracy and assess the influence of:

- Galaxy and PSF characteristics included in the images (size, signal-to-noise, etc.)
- Denoising with the DWT-Wiener algorithm

The quality factors scored for each individual image set are plotted on the left-hand side part of Fig. 2, for each *gfit* variant. They are also quoted in Tables A.1 and A.2.

Due to an editorial mistake, the shear power spectra attributed to “gfit” in the GREAT10 Galaxy Challenge paper, Figure E9, is that from the “fit2-unfold” method. The correct picture was made available at the time of publication and can be found here. We also provide the correct figure in Fig. B.1. We

include the “gfit den” power spectrum in Fig. B.2 as well.

We focus first on the influence of galaxy and PSF features on accuracy. We leave aside the effects of DWT-Wiener denoising for now and thus base our analysis on the results of the “gfit” variant which is devoid of built-in denoising scheme. The data of interest are summarized in Figs. 2 and B.1 and in Tables A.1, A.2.

##### 4.2.1. Influence of Galaxy and PSF characteristics

- **Influence of signal-to-noise ratio:** this is best reflected on the results of the “gfit” variant, since it has no built-in noise correction scheme. All that was done regarding noise was to cut out galaxy and PSF postage stamps to lower dimensions:  $12 \times 12$  pixels for the PSF and  $24 \times 24$  pixels for galaxies. As expected, higher  $S/N$  yields higher Q factors: we observe a roughly linear progression with a  $\sim$  two-fold increase from low  $S/N = 10$  to fiducial  $S/N = 20$  and a  $\sim$  three-fold increase from low  $S/N = 10$  to higher  $S/N = 40$  (see sets 4 to 12 in Fig. 2).
- **Influence of galaxy size:** as seen from the results of sets 13 to 18 in Fig. 2), “gfit” seems quite sensitive to galaxy size, the worst Q factors being obtained on smaller galaxies and the best on the larger ones, with a factor  $\sim 2$  difference. The use of postage stamp cut-outs of identical dimensions, regardless of the actual FWHM of the galaxy they contain could be responsible for this effect, as cut-outs with smaller galaxies are likely to be more noise-dominated than those with larger objects. It may also be that the minimizer is less accurate on smaller objects. “Smooth” galaxies have sizes varying according to a Rayleigh distribution (Kitching et al. 2012), so it is not surprising that the Q factors of the corresponding sets 10, 11, 12 take values in between those

of small and large galaxies.

- **Influence of bulge/disc distribution and offset:** having varying b/d ratios (sets 21, 22) seems to decrease accuracy down to the level of small-size galaxies (sets 13, 14). On the other hand, introducing a non-zero 50/50 bulge-to-disc (b/d) offset (sets 21, 22) tends to yield slightly higher accuracy compared to “smooth” galaxies (sets 17, 18). So it seems the single-component galaxy model (see Sect. 2.3) of “gfit” is more sensitive to b/d ratio than to b/d separation. The use of a more sophisticated galaxy model would certainly yield a small gain for some types of galaxies but at the price of an additional computational time for model fitting. On real data, the importance of the b/d distribution and offset will probably depend on the available galaxy sample.
- **Influence of turbulence:** The raw Q factor plot in Fig. 2 does not show a strong impact from the inclusion of a Kolmogorov power spectrum in the PSF ellipticities. We note however a higher score on the fiducial turbulent set compared to the non-turbulent one for no obvious reason. This seems counter intuitive as PSF turbulence usually degrades accuracy and this phenomenon may actually not be related to turbulence.
- **Influence of spatial variability between images:** as described in Kitching et al. (2012), the Galaxy challenge data are divided into so-called “Single epoch”, “Multi-epoch” and “Stable single epoch” depending on whether the intrinsic ellipticities and PSF keep the same or change their spatial distribution between images in a set (see Table 1). It seems that having fixed instead of variable intrinsic ellipticities (“Multi-epoch” sets) slightly decreases accuracy. Apart from this, no clear trend really stands out from the results and it is not clear whether the difference in accuracy is due to the type of spatial variability used or to the specific sample of images chosen for a set. This topic nevertheless deserves to be investigated further in a separate work.

#### 4.2.2. Effect of denoising on accuracy

We discuss in this section the effect on accuracy of the application of the DWT-Wiener denoising scheme described in Sect. 2.7. The influence of denoising can be clearly observed by comparing the plot of “gfit den” (left) with that of “gfit” in Fig. 2 (right). The corresponding scores are also listed in Tables A.1 and A.2.

We find an average two-fold increase in accuracy, the effect being stronger on high S/N images and larger galaxies. Sets with small galaxies are only slightly improved, however. We also notice that the plots of “gfit” and “gfit den” show identical quality factors for low S/N sets 4 to 6. Further investigation showed that denoising was, by mistake, not applied on those sets. This would probably have improved the overall Q factor of “gfit den”.

These results strongly suggest that the DWT-Wiener algorithm really improves the overall accuracy on galaxy shape measurement. We also note that denoising does not alter the quality factor hierarchy between sets: the sets with best scores in the “gfit” plots remain the same in the “gfit den” plot.

#### 4.3. Bias analysis

We investigate in this section how multiplicative and additive biases are affected by galaxy properties and the use of denoising.

##### 4.3.1. Influence of Galaxy and PSF characteristics

To complement the results of Table 3 relative to bias, we have plotted in Figs. 3 and 4 the multiplicative and additive biases of each set. As noted in Sec. 4.1, “gfit den” reached the lowest average additive bias and the second lowest average multiplicative bias of all 12 twelve competing methods.

Focusing on the multiplicative bias and leaving aside the effect of denoising for now, we can make a few observations from the left-hand side plot of Figs. 3.

- **Highest and lowest multiplicative bias:** all multiplicative bias values, except one (set 5), lie below  $\mathcal{M}/2 = 3.5 \times 10^{-2}$  in absolute value. The largest biases are found on fiducial set 1 (fixed PSF & variable ellipticities), set 5 (low S/N, fixed PSF) and set 18 (smooth galaxies, fixed PSF). The smallest biases are obtained on set 4 (low S/N, fixed PSF & variable ellipticities), set 17 (smooth galaxies, fixed PSF) and sets 22 to 24 (galaxies with varying b/d ratios and fixed PSF, galaxies with non-zero b/d offset).
- **Influence of signal-to-noise ratio:** the results from sets 1 and 7 suggest, as expected, that multiplicative bias decreases with S/N. The low S/N set 4, however, shows a very small bias. It may be that the true bias is large and positive but that it was offset by e.g. a negative bias due to the contribution of large galaxies in that particular set. The relatively large bias of set 5 compared to sets 4 and 6 may also be a consequence of the PSF having a fixed variation pattern in that set.
- **Influence of galaxy size:** small galaxies (sets 13, 14) and large galaxies (sets 15, 16) have comparable biases in absolute value, smaller galaxies having a positive bias and larger ones a negative bias. A lower bias is reached on “Smooth” galaxy images (set 17), likely because the negative and positive biases of small and large galaxies respectively compensate each others. The bias in set 18 may also have been artificially amplified by the fixed variation pattern of the PSF in that set.
- **Influence of bulge/disc distribution and offset:** letting the b/d ratios of galaxy vary within a set tends to yield a multiplicative bias comparable to that of small-size galaxies, probably causing the decrease in accuracy mentioned in Sect. 4.2. In contrast, the biases associated with a non-zero 50/50 b/d offset are among the lowest. As noted earlier, the underlying single-component Sérsic-based galaxy model of “gfit” (see Sect. 2.3) seems handle quite well profiles with an off-centered bulge and disk.
- **Influence of turbulence:** the introduction of PSF with turbulent ellipticities (set 19) does not induce a particularly significant bias compared to the average.
- **Influence of spatial variability between images:** we note that having “Fixed PSF” and “Fixed intrinsic ellipticity” significantly alters the multiplicative bias, especially on low S/N and smooth galaxy sets. Because all images have the

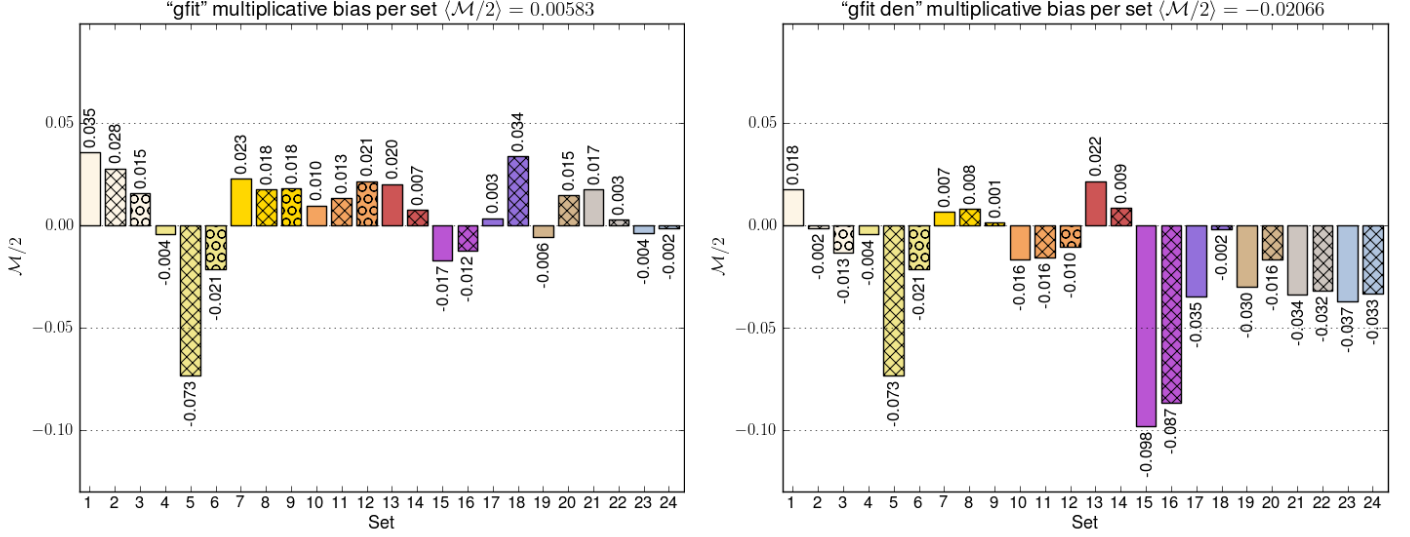


**Fig. 3.** Multiplicative bias  $\mathcal{M}/2$  per set. The legend patterns and colors are identical to those of Fig. 2

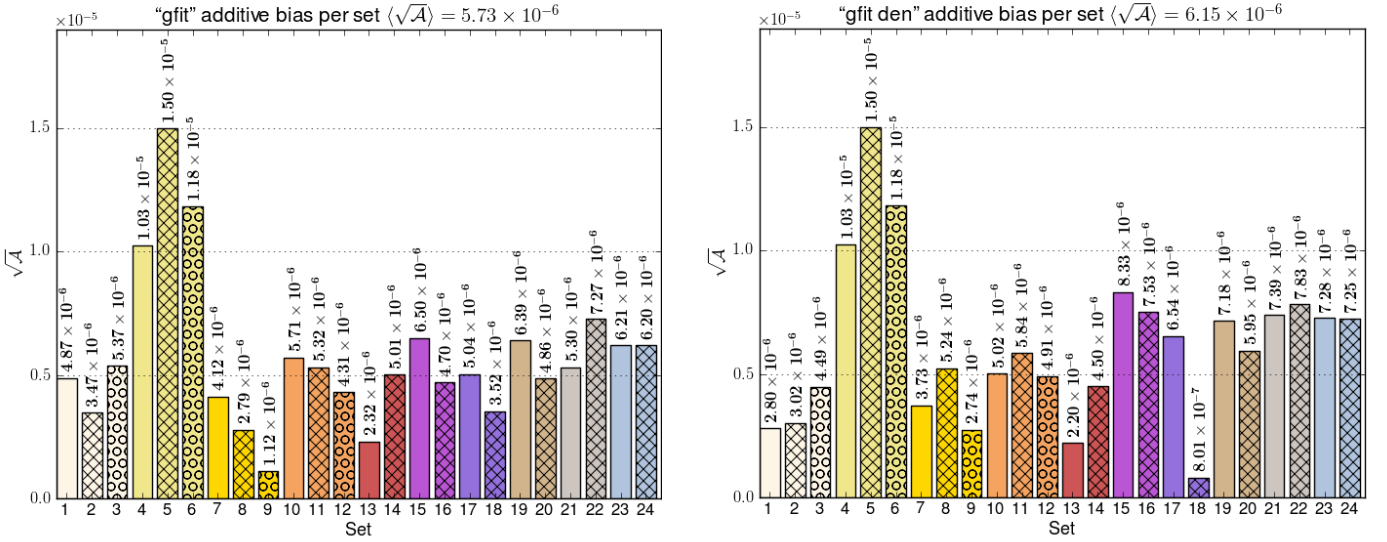


**Fig. 4.** Additive bias  $\sqrt{\mathcal{A}}$  per set. The legend patterns and colors are identical to those of Fig. 2

same spatial variation within a set, it is likely that the bias of one image is just amplified as many times as there are images (i.e. 200 times). The effect is particularly strong on image with low S/N (set 5) and smooth galaxies (set 18).

As far as additive bias is concerned, we note the following trend:

- **Highest and lowest additive bias:** “gfit” obtains an additive bias  $\sqrt{\mathcal{A}} \lesssim 10^{-5}$  on all types of sets, except on the low S/N ones. All values are positive. The lowest bias is reached on small galaxies (sets 13, 14) and the largest on low S/N images (sets 4 to 6).
- **Influence of signal-to-noise ratio:** as for multiplicative bias, we find a trend toward higher biases for lower S/N (sets 1 to 9).
- **Influence of turbulence:** the introduction of a Kolmogorov power spectrum in PSF ellipticity induces a slightly greater additive bias than average (see set 19).

- **Influence of galaxy size:** as for multiplicative bias, we note a tendency of smaller galaxies to have a higher additive bias, as reflected by the values for sets 15 to 18.

- **Influence of bulge/disc distribution and offset:** the additive bias appears larger on galaxies with varying b/d ratios (sets 21, 22) and non-zero b/d offset (sets 23, 24).

#### 4.3.2. Effect of denoising on bias

Comparing the plots for “gfit” and “gfit den” in Figs. 3 and 4, we find that the additive bias does not change significantly, keeping about the same bias values per set. In contrast, the structure of the multiplicative plots is significantly altered.

As seen on the “gfit den” plot, denoising tend to introduce some amount of negative multiplicative bias on all sets. Although the amount of bias on fiducial sets remains roughly the same in absolute value, the DWT-Wiener algorithm clearly impacts the multiplicative bias relative to galaxy size, b/d ratio and turbulence.

As regards galaxy size, even though the multiplicative bias on small galaxies is almost unchanged, that on large galaxies increases about six-fold. Because of that, the bias on “Smooth” galaxies, which also includes large galaxies, also increases.

DWT-Wiener denoising seems to also improve the resolution of the bulge and disk components, so that “gfit” has more difficulty fitting its underlying single-component Sérsic model to images with “uniform” and “offset” b/d. The effect is stronger on larger galaxies, causing a  $\gtrsim$  tenfold multiplicative bias increase.

Lastly, the introduction of PSF turbulence result in a  $\sim$  five-fold multiplicative bias degradation.

Despite the degradation of multiplicative bias on some sets, the accuracy of shape measurements increases two-fold as shown by the corresponding gain in Q factor. We also note that denoising improves the results on sets that already have a high S/N. All in all, the use of denoising is thus clearly beneficial.

## 5. Conclusions

We have described in this paper the *gfit* shape measurement method, a model-fitting based on a simple Sérsic galaxy model (Sect. 2). The method uses a custom-developed minimizer based on a “coordinate descent” algorithm that finds a local minimum with the lowest  $\chi^2$  of the residuals between true and modeled galaxy.

We have also performed an analysis of our results in the GREAT10 Galaxy Challenge (Sect. 3). We participated in the competition with two *gfit* variants: “gfit den”, which applied a denoising step before performing model-fitting, and “gfit”, which did not use denoising. The noise removal technique employed is DWT-Wiener, a wavelet-based, shape-preserving algorithm particularly suitable for shape measurement. (see Sect. 2.7).

We highlight below the main conclusions of your analysis.

- **Method accuracy:** accuracy improves significantly as S/N gets higher and galaxy size larger. The underlying simple Sérsic-based galaxy model of *gfit* has more difficulty handling galaxies with a non-zero 50/50 offset between bulge and disc. The inclusion of Kolomogorov turbulence in ellipticities is not seen to yield a significant change in accuracy.
- **Additive and multiplicative bias:** the non-denoised “gfit” variant reached the lowest average additive bias and second lowest average multiplicative bias of all twelve competing methods. Both additive and multiplicative bias tend to be larger on galaxies with high S/N, smaller size and galaxies with b/d ratio differing from 50/50.
- **Impact of denoising:** the application of the DWT-Wiener noise removal algorithm yields a two-fold improvement in accuracy (Q factor) despite significantly degrading the multiplicative bias on galaxies with a high S/N, small size and significant bulge/disk ratio and separation.

It is interesting to see that, despite the simplicity of the galaxy model used, its results in the Galaxy Challenge established *gfit* as one of the four top-performing methods, both in terms of accuracy and bias. Given that the results were obtained on simulated data, this raises the question of how important having a realistic galaxy model really matters when measuring

galaxy shapes from real data. Providing more clues on this question is one of the objectives of the forthcoming GREAT3 challenge.

*Acknowledgements.* This work is supported by the Swiss National Science Foundation (SNSF). Many thanks to Tom Kitching for his help and for sharing the shear analysis code. We also thank the GREAT10 Coordination Team for organizing this stimulating challenge. GREAT10 was sponsored by a EU FP7 PASCAL 2 challenge grant. We also acknowledge support from the International Space Science Institute (ISSI) in Bern, where some of this research has been discussed.

## References

- Abramowitz, M. & Stegun, I. A. 1965, Handbook of Mathematical Functions, 1st edn., Dover books on mathematics (Dover Publications)
- Anderson, E., Bai, Z., Dongarra, J., et al. 1990, in Proceedings of the 1990 ACM/IEEE conference on Supercomputing, Supercomputing '90 (Los Alamitos, CA, USA: IEEE Computer Society Press), 2–11
- Arce, G. 2005, Nonlinear Signal Processing: A Statistical Approach, Wiley InterScience online books (Wiley-Interscience)
- Arias-Castro, E. & Donoho, D. L. 2009, The Annals of Statistics, 37, 1172
- Bacon, D. J., Refregier, A. R., & Ellis, R. S. 2000, ApJS, 318, 625
- Bartelmann, M. & Schneider, P. 2001, Phys. Rep., 340, 291
- Bernstein, G. M. & Jarvis, M. 2002, AJ, 123, 583
- Bertin, E. & Arnouts, S. 1996, A&AS, 117, 393
- Bonnans, J. F., Gilbert, Lemaréchal, C., & Sagastizábal, C. 2006, Numerical Optimization – Theoretical and Practical Aspects, Universitext (Springer Verlag, Berlin)
- Bridle, S., Balan, S. T., Bethge, M., et al. 2010, MNRAS, 405, 2044
- Bridle, S., Shawe-Taylor, J., Amara, A., et al. 2008, ArXiv eprints, 3, 11
- Bruce, A. G., Donoho, D. L., Gao, H.-y., & Martin, R. D. 1994, Denoising and Robust Non-Linear Wavelet Analysis, Vol. 2242, 325–36
- Ciotti, L. 1991, A&A, 249, 99
- Ciotti, L. & Bertin, G. 1999, Astronomy & Astrophysics, 3, 2
- Community, S. 2010, October, 1
- Forum, M. P. I. 1995, Message Passing Interface Forum
- Forum, M. P. I. 1998, International Journal of High Performance Computing Applications, 12, 1
- Graham, A. W. & Driver, S. P. 2005, Publications of the Astronomical Society of Australia, 22, 11
- Heymans, C., Van Waerbeke, L., Bacon, D., et al. 2006, MNRAS, 368, 1323
- Hirata, C. & Seljak, U. 2003, MNRAS, 343, 459
- Hoekstra, H., Franx, M., Kuijken, K., & Squires, G. 1998, ApJ, 504, 636
- Hoekstra, H. & Jain, B. 2008, Annual Review of Nuclear and Particle Science, 58, 99
- Huterer, D. 2010, General Relativity and Gravitation, 42, 2177
- Huterer, D., Takada, M., Bernstein, G., & Jain, B. 2006, MNRAS, 366, 101
- Jones, E., Oliphant, T., Peterson, P., et al. 2001–, SciPy: Open source scientific tools for Python
- Kaiser, N., Squires, G., & Broadhurst, T. 1995, ApJ, 449, 460
- Kaiser, N., Wilson, G., & Luppino, G. A. 2000, arXiv:astro-ph/0003338
- Khiredine, A., Benmahammed, K., & Puech, W. 2007, Adv. Eng. Softw., 38, 513
- Kitching, T., Amara, A., Gill, M., et al. 2011, Ann.Appl.Stat., 5, 2231
- Kitching, T. D., Balan, S. T., Bridle, S., et al. 2012, MNRAS, 423, 3163
- Kitching, T. D., Miller, L., Heymans, C. E., van Waerbeke, L., & Heavens, A. F. 2008, MNRAS, 390, 149
- Levenberg, K. 1944, The Quarterly of Applied Mathematics, 2, 164
- Luppino, G. A. & Kaiser, N. 1997, ApJ, 475, 20
- Maoli, R., Van Waerbeke, L., Mellier, Y., et al. 2001, A&A, 368, 766
- Marquardt, D. W. 1963, Journal of the Society for Industrial and Applied Mathematics, 11, 431
- Massey, R., Heymans, C., Bergé, J., et al. 2007, MNRAS, 376, 13
- Miller, L., Kitching, T. D., Heymans, C., Heavens, A. F., & van Waerbeke, L. 2007, MNRAS, 382, 315
- Munshi, D., Valageas, P., van Waerbeke, L., & Heavens, A. 2008, Phys. Rep., 462, 67
- Nelder, J. A. & Mead, R. 1965, The Computer Journal, 7, 308
- Nocedal, J. & Wright, S. 1999, Numerical Optimization, Springer Series in Operations Research (Springer)
- Nurbaeva, G., Courbin, F., Gentile, M., & Meylan, G. 2011, A&A, 531, 144
- Nurbaeva, G., Courbin, F., Gentile, M., & Meylan, G. in prep.
- Patil, A., Huard, D., & Fonnesbeck, C. J. 2010, Journal Of Statistical Software, 35, 1

- Powell, M. 1964, The Computer Journal, 7, 155
- Refregier, A. & Bacon, D. 2003, MNRAS, 338, 48
- Sérsic, J. L. 1968, Cordoba
- Tewes, M., Cantale, N., Courbin, F., Kitching, T., & Meylan, G. 2012, A&A, 544, A8
- Trujillo, I., Erwin, P., Ramos, A. A., & Graham, A. W. 2004, Camera, 127, 1917
- Van Waerbeke, L., Mellier, Y., Erben, T., et al. 2000, A&A, 358, 30
- Vetterli, M. & Kovacevic, J. 1995, Wavelets and Subband Coding (Prentice Hall Signal Processing Series) (Prentice Hall PTR)
- Wiener, N. 1949, Extrapolation, Interpolation, and Smoothing of Stationary Time Series (MIT Press)
- Wittman, D. M., Tyson, J. A., Kirkman, D., Dell'Antonio, I., & Bernstein, G. 2000, Nature, 405, 143
- Zhu, C., Byrd, R. H., Lu, P., & Nocedal, J. 1997, ACM Transactions on Mathematical Software, 23, 550

**Table A.1.** “*gfit*”: results per set. Sets with S/N 10, 40 are respectively highlighted in orange and blue. Fiducial sets with S/N 20 are represented in green and all remaining sets also have a S/N of 20.

Set	$Q$	$Q_{dn}$	$Q_{dn \& \text{train}}$	$M/2 \times 10^{-2}$	$\sqrt{\mathcal{A}} \times 10^{-4}$
1	28.26	50.44	205.57	+3.542	+0.0487
2	41.98	78.50	352.54	+2.770	+0.0347
3	31.60	77.86	411.57	+1.539	+0.054
4	17.01	38.11	114.55	-0.432	+0.103
5	18.71	34.41	89.59	-7.345	+0.150
6	14.95	31.32	63.61	-2.136	+0.118
7	100.75	450.35	111.06	+2.270	+0.041
8	120.18	308.43	143.61	+0.176	+0.028
9	82.27	185.17	184.27	+1.780	+0.011
10	39.72	89.40	319.88	+0.964	+0.057
11	35.49	81.86	357.68	+1.327	+0.053
12	35.74	86.16	348.86	+2.141	+0.043
13	48.10	121.62	215.05	+2.010	+0.023
14	44.70	114.73	254.17	+0.740	+0.050
15	72.48	155.84	193.04	-1.732	+0.065
16	87.13	245.81	135.62	-1.238	+0.047
17	52.88	125.30	246.64	+0.334	+0.050
18	44.95	117.64	180.68	+3.366	+0.035
19	58.01	113.55	284.16	-0.593	+0.064
20	44.52	90.47	436.67	+1.465	+0.049
21	39.32	73.23	291.54	+1.732	+0.053
22	35.65	67.33	345.03	+0.271	+0.073
23	54.12	105.81	339.60	-0.382	+0.062
24	54.15	102.45	372.16	-0.164	+0.062
All	50.11	122.74	249.88	+0.583	+0.057

**Table A.2.** “*gfit den*”: results per set. Sets with S/N 10, 40 are respectively highlighted in orange and blue. Fiducial sets with S/N 20 are represented in green and all remaining sets also have a S/N of 20.

Set	$Q$	$Q_{dn}$	$Q_{dn \& \text{train}}$	$M/2 \times 10^{-2}$	$\sqrt{\mathcal{A}} \times 10^{-4}$
1	56.20	182.89	269.98	+1.761	+0.028
2	96.00	316.69	291.60	-0.154	+0.030
3	61.98	271.56	272.04	-1.321	+0.045
4	17.01	38.11	59.06	-0.432	+0.103
5	18.71	34.41	54.09	-7.345	+0.150
6	14.95	31.32	45.34	-2.136	+0.118
7	251.08	518.17	143.08	+0.671	+0.037
8	471.69	203.29	108.09	+0.821	+0.052
9	204.28	503.64	156.95	+0.137	+0.027
10	83.59	303.87	269.16	-1.647	+0.050
11	62.04	162.31	285.93	-1.556	+0.058
12	68.65	258.49	412.10	-1.022	+0.049
13	51.27	165.24	259.73	+2.166	+0.022
14	45.73	127.28	258.15	+0.863	+0.045
15	101.04	100.83	85.12	-9.790	+0.083
16	98.26	101.14	94.13	-8.678	+0.075
17	122.36	207.82	266.86	-3.468	+0.065
18	108.10	264.72	204.89	-0.202	+0.008
19	98.59	154.86	286.79	-0.301	+0.072
20	91.17	198.34	548.31	-1.640	+0.059
21	93.58	158.18	257.46	-3.363	+0.074
22	71.84	137.44	327.12	-3.189	+0.078
23	97.43	144.90	265.60	-0.037	+0.073
24	105.79	163.57	278.86	-3.339	+0.072
All	103.81	197.88	229.19	-2.067	+0.061

## Appendix A: Accuracy and bias per set

Tables A.1 and A.2 respectively quote the actual quality factor and bias values reached by the non-denoised and denoised variants of the *gfit* shape measurement method.

## Appendix B: Sear power spectra

Figs B.1 and B.2 respectively show the shear power spectra of the non-denoised and denoised variants of *gfit* submitted in the GREAT10 galaxy Challenge.

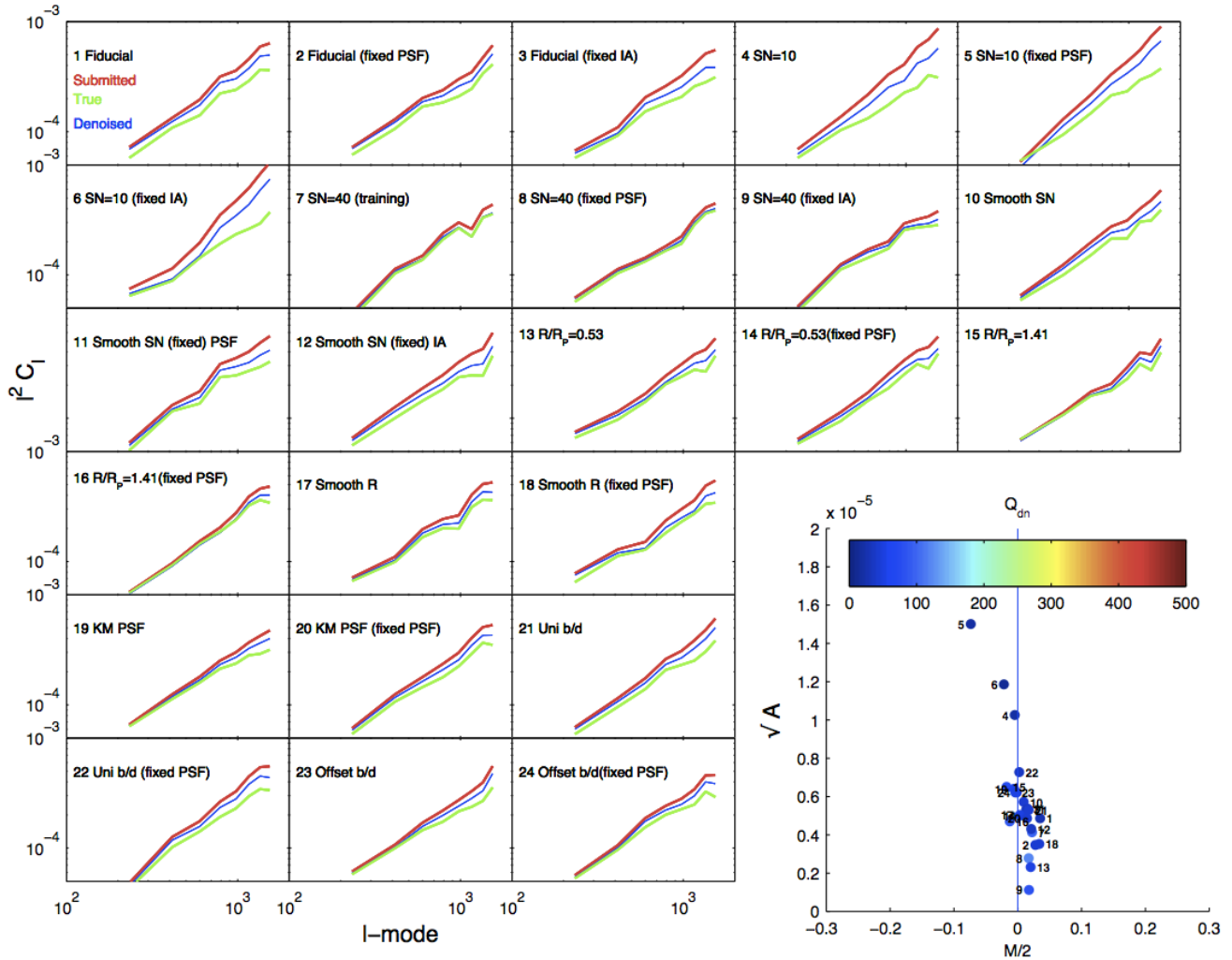


**Fig. B.1.** The shear power spectra of the “*gfit*” variant over the 24 sets of the Galaxy challenge. The red lines denote the estimated shear power spectra while the green lines represents the true shear power. The blue lines indicate the spectra after application of pixel-level denoising (not DWT-Wiener denoising). The code run to plot these power spectra is identical to that used in the (Kitching et al. 2012) paper. Note that the power spectra attributed to “*gfit*” in the Figure E9 of (Kitching et al. 2012) are actually those of the “*fit2-unfold*” method.

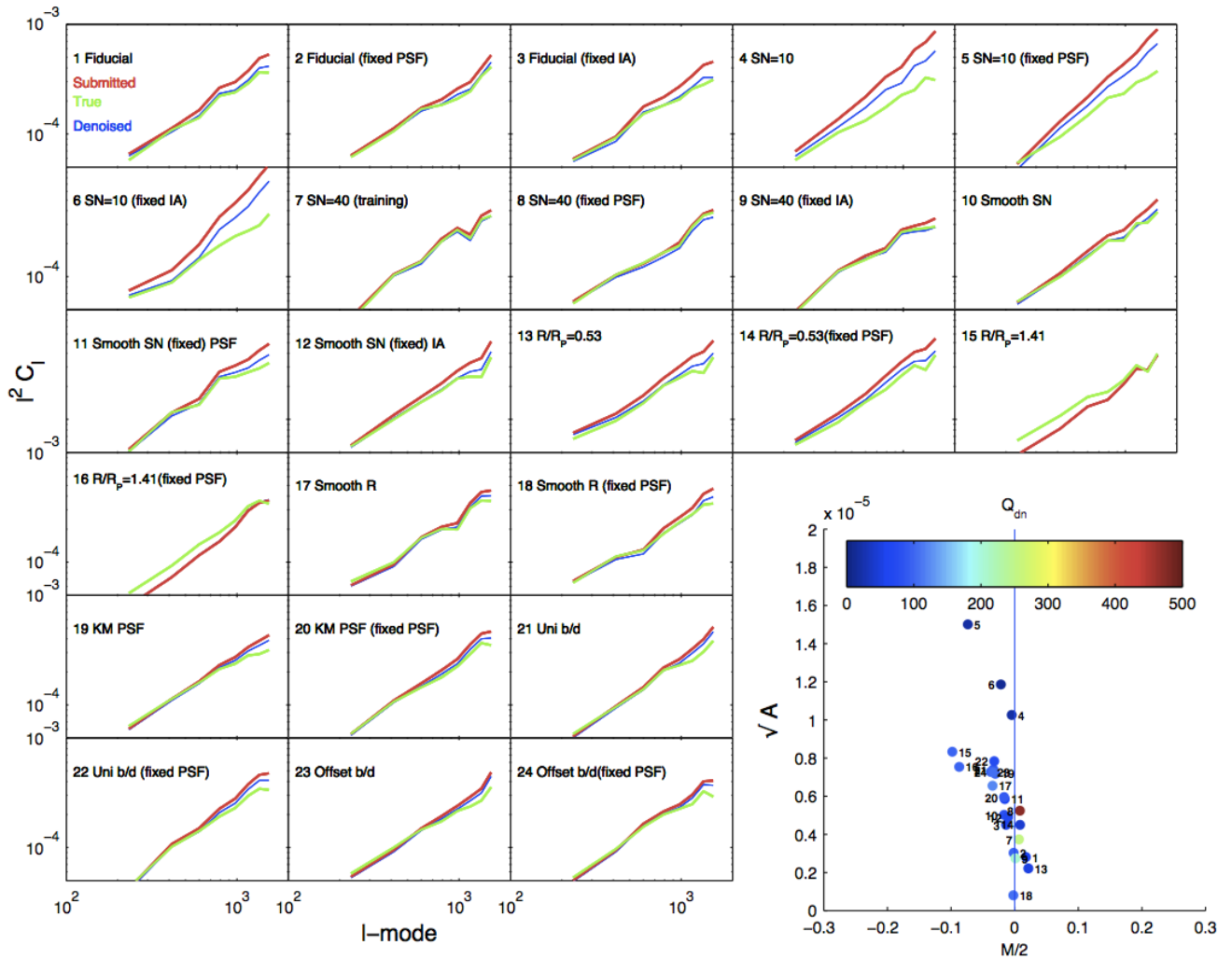


**Fig. B.2.** The shear power spectra of the “gfit den” variant over the 24 sets of the Galaxy challenge. This variant has a preliminary denoising step using the DWT-Wiener algorithm. The red lines denote the estimated shear power spectra while the green lines represents the true shear power. The blue lines indicate the spectra after application of pixel-level denoising (not DWT-Wiener denoising). The code run to plot these power spectra is identical to that used in the (Kitching et al. 2012) paper.